Cartesian Inertia Optimisation via Redundancy Resolution for Physical Human Robot Interaction

Sheila Sutjipto, Jon Woolfrey, Marc G. Carmichael and Gavin Paul

***Abstract*— The objective of introducing robotic manipulators into human-centric domains is to improve the efficacy of tasks in a safe and practical manner. The shift toward collaborative manipulator platforms has facilitated physical human-robot interaction (pHRI) in such environments. Often, these platforms are kinematically redundant and possess more degrees of freedom (DOF) than needed to complete a desired task. When no additional task is defined, it is possible for the manipulator to converge upon joint configurations that are unfavourable for the collaborative task. Consequently, there is potential for the posture of the manipulator to affect the interaction experienced. This paper investigates an inertia-based optimization control method for redundant manipulators interacting with an active agent. The inertia-based reconfiguration is evaluated through simulations and quantified with real-life experiments conducted with a robot-robot dyad. It was found that resolving redundancy to reconfigure the Cartesian inertia reduced the energy expenditure of the active agent during the interaction.**

I. INTRODUCTION

In robotics, the purpose of a manipulator is to act upon or interact with the external world, whether it be the environment, other robots, or humans. Although precise motions have traditionally been a cornerstone of industrial robots, the shift towards working in unstructured and dynamic environments has required robots to be safer, reactive to their surroundings, and compliant to the interaction forces experienced. These characteristics can be achieved through compliant control. Two fundamental methods used to achieve compliant behaviour are impedance and admittance control, which are reciprocals of each other [1]. The premise of these control methods involves designing a compliant profile, generally defined as a mass-spring-damper model. During such interactions, the focus has shifted to the modulation of interaction forces rather than the execution of precise motions.

For physical human-robot interaction (pHRI), there is an increasing trend for the regulation of interaction forces during external contact to facilitate a stable interface for creating cooperative interactions. To achieve this, studies have focused on modulating behaviour defining parameters (stiffness and damping) based upon human characteristics of point-to-point motions and minimum jerk trajectories [2]; improve carrying and positioning performance of a co-manipulated object through stiffness modulation [3]; and mimicking impedance profiles of experts [4].

Although it is possible to solely manipulate control parameters to embody a compliant profile, research has shown that a robot's capability for facilitating stiffness is fundamentally linked to the geometry that is exhibited. This knowledge has been leveraged to improve the desired robot behaviour [5]. Interestingly, in [6] it was postulated that a relationship exists between maximizing the stiffness of the end-effector along a direction and minimizing the joint torques of a robot given an externally applied force. Conversely, applying these techniques to pHRI can enable compliant robot behaviour (minimizing stiffness), to facilitate ease of motion when co-manipulating an object with a human or another robot.

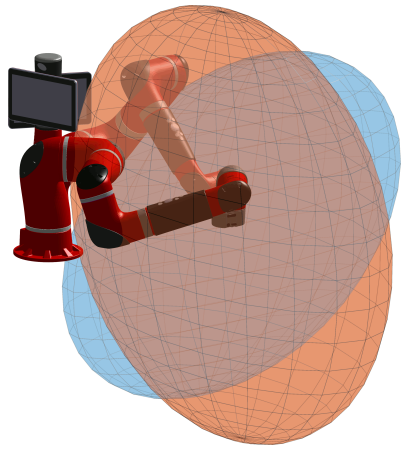

Fig. 1: Two poses with their respective inertia ellipsoids for maximum (blue) and minimum (orange) inertial effects during interaction.

In addition to designing stiffness and damping matrices to achieve a desired impedance, it is also possible to alter the desired inertial behaviour of the system. For example, with manipulators acting as rehabilitative devices, resistance training exercises can be improved by increasing the apparent inertia at the end-effector, this can be beneficial since collaborative robots are not as physically capable as their industrial counterparts [7][8]. However, modulating the inertial behaviour is comparatively more limiting since a measurement of the external forces is required, and external forces may not necessarily act on the end-effector of the robot [9]. Subsequently, rather than designing the inertial behaviour of the end-effector through control parameters, there is a need to investigate the effect of arm postures on the apparent inertia. A notable difference between two different Cartesian inertia ellipsoids is shown in Fig. 1. This highlights the effect of dropping the elbow joint of the manipulator for inertia reshaping.

The notion of incorporating inertial properties has been

The authors are with the Centre for Autonomous Systems (UTS:CAS), University of Technology Sydney (UTS), Sydney, Australia. Corresponding author email: sheila.sutjipto@uts.edu.au

used for the design of manipulators [10] and minimizing impulsive forces during robot-environment collisions [11]. Similarly, [12] proposes an approach to minimise impulsive forces present during the initial contact between a manipulator and a free floating object. Since free floating manipulators and objects are unable to absorb reaction forces, there is potential for impulsive forces at contact to cause either party to float away, requiring additional energy to be expended for reducing the introduced error and stabilising the platform.

Humans can distinguish between different interactions based on the designed controller, like the experience of shaking another person's hand [13], or when applying singularity avoidance strategies for pHRI [14]. Consequently, it is evident that shaping the apparent inertia can have an effect on the pHRI experience. During a co-manipulation task, [15] reconfigures the arm such that the apparent inertia is close to an isotropic ellipse. This attempts to ensure that the end-effector of the robot *feels* similar in all directions of movement. Additionally inertia shaping has been employed for minimizing contact forces for haptic devices and impedance controlled robots [16]. This is particularly relevant for platforms with large workspaces, since the non-linearity of the end-effector behaviour and apparent inertia affects the perception of the interaction by the human. Furthermore, shaping the apparent inertia can be leveraged to minimise the interaction forces experienced, and thus the work done by the human.

In this paper, an optimization-based approach for inertia reshaping is explored. Understanding how robot joint configurations can affect the interaction is necessary for improving robot behaviours, especially during pHRI where forces exchanged can dictate experience. Consequently, the focus is to investigate the influence of robot configurations on the Cartesian inertia through simulations and experiments. However, since humans show inherent variability, obtaining objective measures is known to be difficult. Thus, a repeatable and precise robot is used for real-world experiments to obtain an unbiased quantitative measure of this effect.

II. PROBLEM FORMULATION

A. Differential Kinematics

The end-effector pose of a serial-link chain can be represented as a function of its joint angles

$$\mathbf{x} = \mathbf{f}(\mathbf{q}) \tag{1}$$

where, $\mathbf{q} \in \mathbb{R}^n$ is a vector of joint angles and $\mathbf{x} \in \mathbb{R}^m$ represents the end-effector pose of the chain. The time derivative of Eqn. (1) describes the following relationship:

$$\begin{aligned} \dot{\mathbf{x}} &= \frac{\partial \mathbf{f}(\mathbf{q})}{\partial \mathbf{q}} \dot{\mathbf{q}} \\ \dot{\mathbf{x}} &= \mathbf{J}(\mathbf{q}) \dot{\mathbf{q}} \end{aligned} \tag{2}$$

Differentiating Eqn. (2), with respect to time gives:

$$\ddot{\mathbf{x}} = \mathbf{J}(\mathbf{q})\ddot{\mathbf{q}} + \dot{\mathbf{J}}(\mathbf{q})\dot{\mathbf{q}} \tag{3}$$

where, $\mathbf{J}(\mathbf{q}) \in \mathbb{R}^{m \times n}$ is the Jacobian matrix of the manipulator at a given joint configuration.

B. Redundancy Resolution

If $\mathrm{rank}(\mathbf{J}) = m < n$, the system is considered redundant, thus possessing infinite joint motions, $\ddot{\mathbf{q}}$, that satisfy some desired end-effector motion, $\ddot{\mathbf{x}}$. One proposed approach that utilises redundancy defines a cost function at the velocity level, weighted by the inertia matrix of the manipulator $\mathbf{M}(\mathbf{q}) \in \mathbb{R}^{n \times n}$:

$$\begin{aligned} \min_{\ddot{\mathbf{q}}} \quad & \frac{1}{2}(\ddot{\mathbf{q}} - \ddot{\mathbf{q}}_\mathbf{r})^{\mathrm{T}} \mathbf{M} (\ddot{\mathbf{q}} - \ddot{\mathbf{q}}_\mathbf{r}) \\ \text{s.t.} \quad & \ddot{\mathbf{x}} - \mathbf{J}\ddot{\mathbf{q}} - \dot{\mathbf{J}}\dot{\mathbf{q}} = 0 \end{aligned} \tag{4}$$

The following equation is then obtained from the minimisation using Lagrange multipliers:

$$\ddot{\mathbf{q}} = \mathbf{J}_\mathbf{M}^\dagger (\ddot{\mathbf{x}} - \dot{\mathbf{J}}\dot{\mathbf{q}}) + \mathbf{N}_\mathbf{M} \ddot{\mathbf{q}}_\mathbf{r} \tag{5}$$

where, $\ddot{\mathbf{q}}_\mathbf{r} \in \mathbb{R}^n$ is the the vector of desired joint accelerations for a redundant task, $\mathbf{J}_\mathbf{M}^\dagger = \mathbf{M}^{-1}\mathbf{J}^{\mathrm{T}}\left(\mathbf{J}\mathbf{M}^{-1}\mathbf{J}^{\mathrm{T}}\right)^{-1}$ is the dynamically consistent pseudo-inverse Jacobian, and $\mathbf{N}_\mathrm{M} = (\mathbf{I} - \mathbf{J}_\mathbf{M}^\dagger \mathbf{J})$ is the weighted null space projection matrix.

The redundant task executed in the null space of the robot can be assigned as:

$$\ddot{\mathbf{q}}_\mathbf{r} = \alpha \mathbf{M}^{-1} \nabla \mathrm{c}(\mathbf{q}) \tag{6}$$

where, α is a scalar that dictates whether the cost function acts as a maximization or minimization, and, $\nabla \mathrm{c}(\mathbf{q})$, is the gradient of the cost function that is dependent on the joint configuration of the robot.

C. Dynamics

The dynamical model of the manipulator expressed in joint space is:

$$\mathbf{M}(\mathbf{q})\ddot{\mathbf{q}} + \mathbf{C}(\mathbf{q}, \dot{\mathbf{q}})\dot{\mathbf{q}} + \mathbf{g}(\mathbf{q}) = \boldsymbol{\tau} - \mathbf{J}^{\mathrm{T}}\mathbf{w}_{\mathrm{int}} \tag{7}$$

with $\mathbf{C}(\mathbf{q}, \dot{\mathbf{q}}) \in \mathbb{R}^{n \times n}$ representing the Coriolis and centrifugal matrices, $\mathbf{g}(\mathbf{q}) \in \mathbb{R}^n$ representing the vector of gravitational torques, and $\boldsymbol{\tau}$ and $\mathbf{J}^{\mathrm{T}}\mathbf{w}_{\mathrm{int}}$ are the control and interaction torques respectively. For this work, it is assumed that the gravitational component is compensated for by the robot, and thus omitted from subsequent equations.

Substituting Eqn. (5) into the dynamical model of the manipulator results in the following equation:

$$\boldsymbol{\tau} - \mathbf{J}^{\mathrm{T}}\mathbf{w}_{\mathrm{int}} = \mathbf{J}^{\mathrm{T}}\boldsymbol{\Lambda}(\ddot{\mathbf{x}} - \dot{\mathbf{J}}\dot{\mathbf{q}}) + \mathbf{C}\dot{\mathbf{q}} + \mathbf{N}_\mathbf{M}^{\mathrm{T}}\boldsymbol{\tau}_{\mathrm{r}} \tag{8}$$

where $\boldsymbol{\Lambda}(\mathbf{q}) = (\mathbf{J}\mathbf{M}^{-1}\mathbf{J}^{\mathrm{T}})^{-1}$ is the Cartesian inertia matrix and $\boldsymbol{\tau}_r$ is the redundant torque Multiplying Eqn. (8) through by, $\left(\mathbf{J}_\mathbf{M}^\dagger\right)^{\mathrm{T}}$, leads to the model represented in operational (Cartesian) space [17]:

$$\mathbf{w} - \mathbf{w}_{\mathrm{int}} = \boldsymbol{\Lambda}\ddot{\mathbf{x}} + \boldsymbol{\Lambda}(\mathbf{J}\mathbf{M}^{-1}\mathbf{C} - \dot{\mathbf{J}})\dot{\mathbf{q}} \tag{9}$$

Additionally, the term $\left(\mathbf{J}_\mathbf{M}^\dagger\right)^{\mathrm{T}}\mathbf{N}_\mathbf{M}^\mathbf{T} = \mathbf{0}$, and subsequently the null space torques generated will have no effect on the robot end-effector forces, $\mathbf{w}$. For the end-effector to behave as a mass-spring-damper system, the following is used:

$$\boldsymbol{\Lambda}_\mathrm{d}\ddot{\mathbf{e}} + \mathbf{D}_\mathrm{d}\dot{\mathbf{e}} + \mathbf{K}_\mathrm{d}\mathbf{e} = \mathbf{w}_{\mathrm{int}} \tag{10}$$

where,

- $\mathbf{\Lambda}_\mathrm{d}$ is the desired end-effector inertia,
- $\mathbf{D}_\mathrm{d}$ is the desired damping,
- $\mathbf{K}_\mathrm{d}$ is the desired stiffness,
- $\mathbf{e} = \mathbf{x}_\mathrm{d} - \mathbf{x}$ and its derivatives are the error terms.

Choosing the desired inertia, Λ_d to be the natural apparent inertia forms the following control law:

$$\mathbf{w} = \mathbf{\Lambda}\ddot{\mathbf{x}} + \mathbf{D}_\mathrm{d}\dot{\mathbf{e}} + \mathbf{K}_\mathrm{d}\mathbf{e} + \mathbf{\Lambda}(\mathbf{J}\mathbf{M}^{-1}\mathbf{C} - \dot{\mathbf{J}})\dot{\mathbf{q}} \tag{11}$$

III. METHODS FOR OPTIMAL ARM RECONFIGURATION

Ellipsoidal representations of kinematic and dynamic measures are widely used to determine whether a manipulator is well configured to achieve a desired motion. They provide a graphical representation of kinematic and dynamic measures, aiding intuition when attempting to understand dynamics of complex manipulators.

One measure of interest frequently used for robots in isolation and pHRI is the measure of manipulability [18], with its corresponding ellipsoid defined as:

$$\dot{\mathbf{x}}^\mathrm{T}(\mathbf{J}\mathbf{J}^\mathrm{T})^{-1}\dot{\mathbf{x}} = 1 \tag{12}$$

This definition forms an ellipsoid in $\mathbb{R}^m$, and the volume bounded by the ellipse is used to determine whether a particular manipulator configuration is near singular.

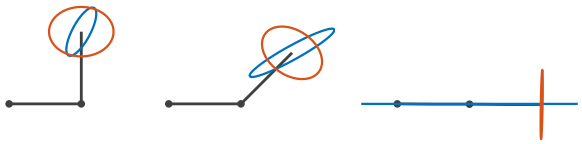

Fig. 2: Three joint configurations of a 2 link planar manipulator illustrating the respective force ellipsoids, $\mathbf{J}\mathbf{J}^\mathrm{T}$, in blue and Cartesian inertia ellipsoids, $(\mathbf{J}\mathbf{M}^{-1}\mathbf{J}^\mathrm{T})^{-1}$, in orange.

A. Cartesian Force Control

When considering a static manipulator, the dynamic model of the manipulator can be reduced to $\boldsymbol{\tau} = \mathbf{J}^\mathbf{T}\mathbf{w}$. By satisfying this constraint $||\boldsymbol{\tau}|| = 1$, a force ellipsoid can be defined as:

$$\begin{aligned} \boldsymbol{\tau}^\mathrm{T}\boldsymbol{\tau} &= 1 \\ \mathbf{w}^\mathrm{T}\mathbf{J}\mathbf{J}^\mathrm{T}\mathbf{w} &= 1 \end{aligned} \tag{13}$$

The eigenvectors and eigenvalues of the inner component of Eqn. (13) describes the shape of the force ellipsoid. Since this component is comprised of the Jacobian, the end-effector force ellipsoid changes as a function of this parameter. Maximizing or minimizing the axes of the force ellipsoid is then defined as:

$$\mathbf{c}(\mathbf{q}) = \frac{\mathbf{1}}{\mathbf{2}}\mathbf{w}^\mathrm{T}\mathbf{J}\mathbf{J}^\mathrm{T}\mathbf{w} \tag{14}$$

$$\frac{\partial \mathbf{c}(\mathbf{q})}{\partial \mathbf{q_i}} = \mathbf{w}^\mathrm{T}\frac{\partial \mathbf{J}}{\partial \mathbf{q_i}}\mathbf{J}^\mathbf{T}\mathbf{w} \tag{15}$$

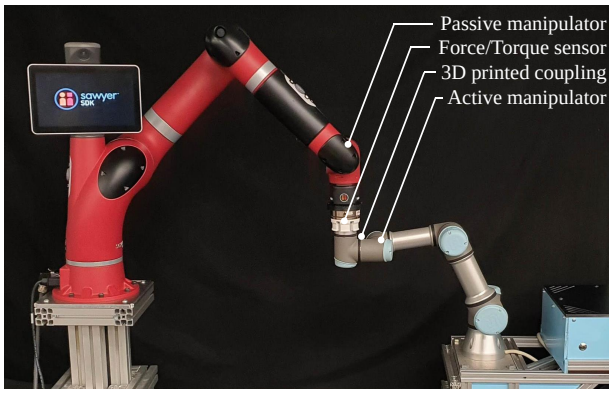

Fig. 3: Setup for physical experiments

The force ellipsoids for a planar uniform 2 link manipulator are shown with blue illustrations in Fig. 2. The result from maximizing the force ellipsoid is associated with the manipulator's ability to generate or sustain increased forces in the optimized direction. As the arm approaches near singular configurations, the ellipsoid can be seen to reduce itself to an infinitely long line. Forces applied along this line can theoretically be infinite since they are directed through the structure of the robot, while forces applied along the minor axis are not conducive to sustaining the same forces.

B. Cartesian Inertia Optimization

An alternate cost function is proposed below which considers the effect of the robot's link masses and inertia which subsequently alters the inertia of the manipulator in Cartesian space. Here, $\mathbf{n} \in \mathbb{R}^m$ is used to specify the desired direction to optimize along.

$$\begin{aligned} \mathbf{c}(\mathbf{q}) &= \frac{\mathbf{1}}{\mathbf{2}}(\mathbf{n}^\mathrm{T}\mathbf{\Lambda}(\mathbf{q})\mathbf{n}) \\ \frac{\partial \mathbf{c}(\mathbf{q})}{\partial \mathbf{q_i}} &= \frac{\mathbf{1}}{\mathbf{2}}\left(\mathbf{n}^\mathrm{T}\frac{\partial \mathbf{\Lambda}(\mathbf{q})}{\partial \mathbf{q_i}}\mathbf{n}\right) \end{aligned} \tag{16}$$

Eqn. (16) enables the manipulator's Cartesian inertia experienced at the end-effector to be directly altered by maximizing or minimizing an axis of the represented ellipsoid by reconfiguring the arm. This approach is akin to the work presented in [11], however the formulation is derived from an impulse-based contact model. Since an impulsive contact model is considered, their findings highlight the instantaneous effects that occur when contacts occur between a manipulator and the environment. In contrast, this work considers the effect of reconfiguring the arm based upon inertia over time and its relationship with energy.

Similar to the force ellipsoids drawn, the Cartesian inertia representation is still susceptible to singular robot configurations as shown in Fig. 2. It is worth noting that although the resulting ellipses from force and inertia optimization appear to be inverses of each other, the inclusion of link masses alters the resulting ellipsoidal representation. The partial derivative of the Cartesian inertia ellipse is then defined as

$$\frac{\partial \mathbf{\Lambda}(\mathbf{q})}{\partial \mathbf{q}} = \mathbf{\Lambda}(\mathbf{q})\left(\mathbf{J}\mathbf{M}^{-1}\frac{\partial \mathbf{M}}{\partial \mathbf{q}} - 2\frac{\partial \mathbf{J}}{\partial \mathbf{q}}\right)\mathbf{J}^\dagger_\mathbf{M} \tag{17}$$

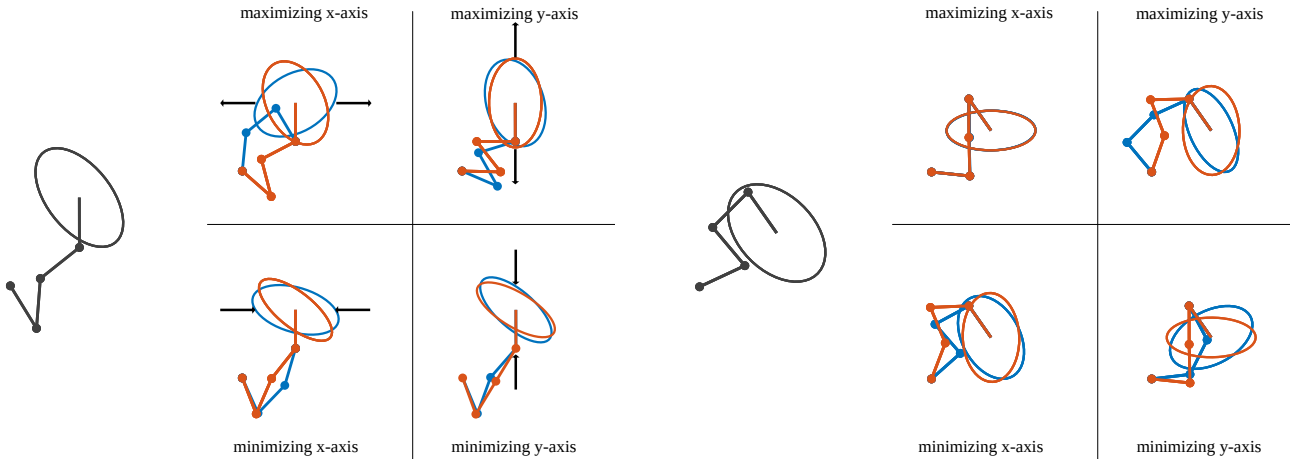

Fig. 4: Four link planar simulation resulting joint configuration from force (blue) and inertia (orange) optimization with Cartesian inertia ellipses. Two examples are shown with random initial configurations (grey).

To optimize the apparent inertia along the desired axis, the null space torques in Eqn. (8), $\boldsymbol{\tau}_{\mathbf{r}} = \alpha \nabla \mathbf{c}(\mathbf{q})$, is set proportional to the cost function. For values where $\alpha < 0$, the arm will rearrange itself to minimise the apparent inertia in the specified direction. Consequently, interactions with the end-effector require less force to achieve increased end-effector acceleration. Conversely when $\alpha > 0$, the arm realigns itself to maximise the apparent inertia, resisting changes from the experienced end-effector accelerations.

IV. APPLICATION OF THE PROPOSED STRATEGY

A. Simulations

To obtain an intuition for the effect of the optimization, the method is applied on a uniform length 4 link planar revolute manipulator. The mass of the links from base to end-effector were selected as 2, 1, 0.5 and 0.25kg respectively. Random joint configurations were selected as the starting configuration for all simulations.

Fig. 4 illustrates four different cases representing each possible parameter combination. From the figure, it is evident optimizing for inertia is not the same as optimizing for force given the final joint configurations that have been converged upon. For the ellipse representation chosen, the major axis indicates the direction with a reduced apparent inertia.

When minimizing the apparent inertia of the manipulator (see Fig. 4, top row of superimposed figures), end-effector motion along the specified axis is easier to achieve as the structure of the arm is conducive to being *compressed* along the specified axis. This generally results in each link's centre of mass (COM) to be situated as close as possible to adjoining links. Alternatively, in Fig. 4b the robot assumes a configuration such that a large moment arm exists about joint 2 reducing the necessary force required to move the end-effector in the x-axis.

Conversely, maximizing the apparent inertia of the manipulator results in structures where external forces on the end-effector are directed through the structure rather than the joints. From Fig. 4 it can be seen that the arm reconfigures itself such that it expands to increase the relative distance between the links' COM. As a result, the manipulator's structure would be better equipped to resist forces along the maximised axis, subsequently making it feel more difficult to move during pHRI. Additionally, it is noted that for Fig. 4a maximizing the x-axis of the Cartesian inertia ellipse is not equivalent to minimizing the y-axis. However, when investigating this effect for Fig. 4b, the configurations converged upon are reciprocals of each other.

The geometries assumed by the planar manipulator, when optimizing based upon Cartesian force, show that the forces experienced at the end-effector are directed through the structure of the robot, rather than the joints. From the derivation it can be seen that this is reasonable since the cost incorporates $\mathbf{J}(\mathbf{q})$, which encompass two physical properties of the manipulator: joint positions and link lengths.

Furthermore, varying the masses of the planar manipulator alters the final configuration that the optimization converges upon. As previously mentioned, since force based optimization techniques are based upon $\mathbf{J}\mathbf{J}^{\mathrm{T}}$, varying the mass will possess no effect on the optimization process. In contrast, as shown in Fig. 4, inertia-based optimization incorporates additional physical from each link to reconfigure the arm.

B. Experiments on a Physical Platform

The examples for a uniform planar robot are well-understood, however, robotic systems prevalent in pHRI applications exhibit complex geometries. Subsequently, these results are intended to provide insight to understand the dynamics of complex manipulators.

To demonstrate the influence of the apparent inertia applied during an interaction, the proposed inertia shaping method is applied on a physical platform. The physical setup consists of two collaborative robots as shown in Fig. 3; a 7DOF Sawyer manipulator (Rethink Robotics) and a 6DOF UR3 manipulator (Universal Robots), where an

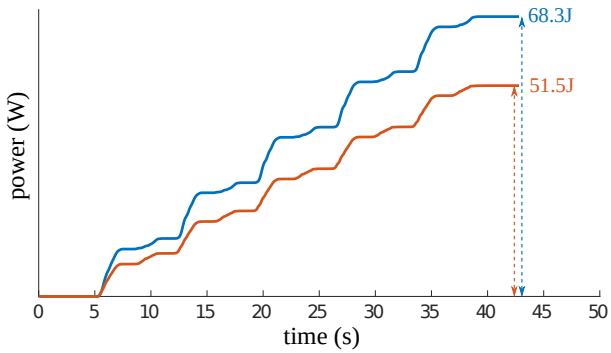

Fig. 5: Cumulative power over the duration of the interaction. The action of moving the Sawyer's end-effector toward the base then away from the base is repeated 5 times.

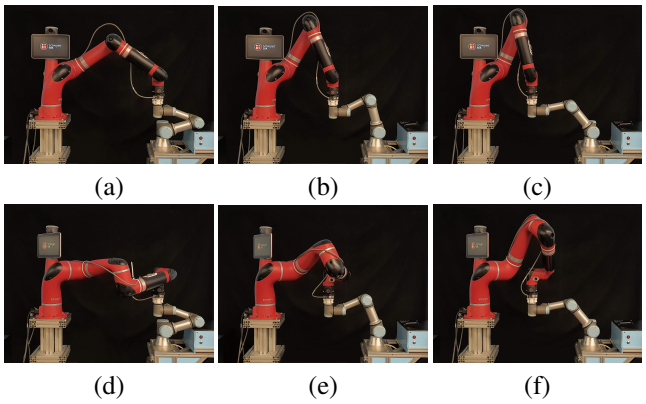

Fig. 6: The proposed control method actively rearranges the manipulator such that the joint configuration assumed is conducive to motion along the x-axis. In (a)-(c) no redundant task is specified, while (d)-(f) shows the optimal Cartesian inertia-based configurations along the trajectory as defined by the cost.

Axia80-M20 (ATI Industrial Automation) was fitted to a 3D printed component and used to secure the two manipulators together. Communication between devices was facilitated by Robot Operating System (ROS). The Sawyer and UR3 were commanded using manufacturer-endorsed ROS packages, intera_sdk and Universal_Robots_ROS_Driver respectively. Since the two systems are independent of each other, the control frequencies chosen for the Sawyer and UR3 were 50Hz and 125Hz.

To ascertain the effect of reconfiguration over the duration of an interaction, the end-effector of the UR3 is moved with a constant acceleration profile to highlight the relationship between the effective mass and acceleration. Using the force-torque sensor and measured end-effector velocities of the Sawyer, the energy expended by the UR3 during the interaction was calculated. A 25% reduction in expended energy was recorded, using $51.452J$ when actively reshaping the Sawyer's apparent inertia instead of the original $68.298J$ without a redundant task specified. Over the course of the repeated interactions, Fig. 5 demonstrates how the energy expended begins to deviate as more repetitions are performed.

V. DISCUSSION

From the simulation and physical experiments, the final joint configurations maintained the same end-effector pose. This demonstrated that the control method did not disturb the primary task of maintaining a desired pose, accomplishing the inertia reshaping in the null space of the manipulator.

A. Physical Platform

When the Sawyer's end-effector is moved along the x-axis closer to the base, a larger force is experienced since the Sawyer is not commanded to actively reconfigure itself. The effect of this larger force corresponds to a larger increase in cumulative power shown when the robot moves from rest for each repetition in Fig. 5. As the end-effector is moving away from the base, the forces experienced are comparable regardless of whether the task for reconfiguration is applied. This is due to the robot converging on joint configurations with the elbow raised as seen in Fig. 6(c) and (f). An increase in the measured force is supported by the values in the Cartesian inertia matrix corresponding to the x-axis. With the postures shown in Fig. 6(a) and (d), the effect of reconfiguration reduces this value from 3.86kg to 2.28kg which is a 40% reduction in the apparent mass.

As previously discussed from the simulations, minimizing the apparent inertia at the end-effector allows the manipulator to alter the COM of its structure. For the particular postures shown in Fig. 6(d)-(f), the joint trajectory exhibited does not require the active party, the UR3, to move the COM of the Sawyer, against gravity, rather the null space task will actively inject joint torques to achieve this.

Consequently, it is evident that although the energy expenditure of the active robot is minimised, the measured robot joint torques can be larger when incorporating the null space task. Since the manipulator is actively rearranging itself such that the human or robot interacting with the end-effector expends less energy, it is reasonable for this result to occur.

Interestingly, since the acceleration profile is constant, the results indicate that the forces experienced at the end-effector are not symmetrical when moving in opposite directions when the null space task is not defined. Other than the resultant joint configuration assumed, another factor contributing to this may include assistive and resistive forces due to gravity when lifting and dropping the elbow joint when the end-effector moves closer and away from the base.

It is also noted that while maintaining the same end-effector pose, it was observed that various starting manipulator postures converge to similar configurations as shown in Fig. 7. In this example, the final configuration has the robot elbow fall towards the negative y-axis. Without considering the inertial properties of the links, it is possible that the elbow of the robot starting at Fig. 7a could fall towards either side of the y-axis. In Fig. 7b, the intuition is that the manipulator is more likely to converge to the positive y-axis since this configuration is closer to the initial state. However, when

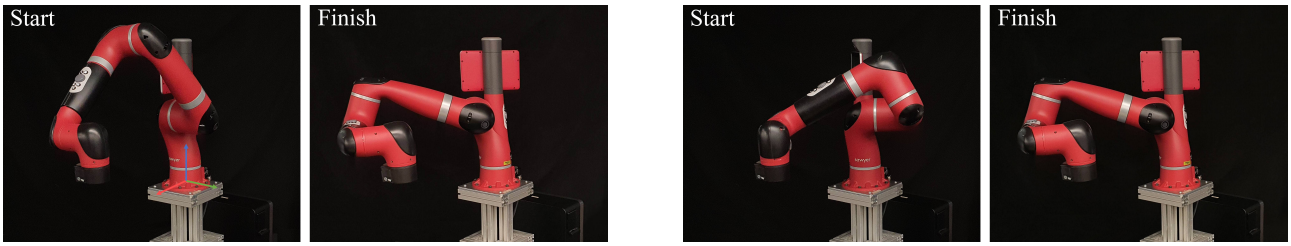

(a) (b)

Fig. 7: Similar joint configurations are converged upon via inertia optimization in the x-axis regardless of the starting joint configuration.

the inertial properties of the manipulator are considered, the resultant configuration forces the elbow into the negative y-axis region. Consequently, it is shown that optimizing for inertia along a particular axis does not necessarily converge to symmetrical configurations.

Similar to the simulation results, the reconfiguration moves the arm's COM such that motion along the x-axis leverages the moment created about the elbow joint, reinforcing the insights from Fig. 7b. This reduces the power required to move the end-effector from rest in the chosen direction.

VI. CONCLUSIONS

During physical human robot interaction, the interaction forces felt by the human will vary depending upon the joint configuration of the manipulator. This non-linear inertial behaviour of the end-effector is measurable and can affect the interaction experienced by the human. This paper has explored the aforementioned effect using inertia shaping to reduce the power required to move the end-effector of a manipulator. The inertia shaping method was evaluated by demonstrating its effect through simulation and on a robot-robot coupled system. In simulation, ellipsoidal representations were used to show how a robot can be reconfigured so that the end-effector inertia is minimized along a desired axis. The method was then applied on a physical platform quantifying the effect of the null space reconfiguration. Results from these experiments indicate that optimizing the end-effector inertia facilitates the reduction of energy expenditure. Although this approach has been shown to reduce the energy expended, further investigation is necessary to determine its impact on the pHRI experience.

ACKNOWLEDGMENT

Sheila Sutjipto is supported by an Australian Government Research Training Program Scholarship. The authors would like to thank Richardo Khonasty and Dinh Tung Le for helping setup the experiments, and to Yujun Lai for giving detailed feedback on the manuscript.

REFERENCES

[1] N. Hogan, "Impedance control: An approach to manipulation: Part I—Theory," *Journal of dynamic systems, measurement, and control*, vol. 107, no. 1, pp. 1–7, 1985.

[2] R. Ikeura and H. Inooka, "Variable impedance control of a robot for cooperation with a human," in *Proceedings - IEEE International Conference on Robotics and Automation*, vol. 3, 1995, pp. 3097–3102.

[3] T. Tsumugiwa, R. Yokogawa, and K. Hara, "Variable impedance control with virtual stiffness for human-robot cooperative peg-in-hole task," in *IEEE International Conference on Intelligent Robots and Systems*, vol. 2, 2002, pp. 1075–1081.

[4] M. S. Erden and A. Billard, "Robotic Assistance by Impedance Compensation for Hand Movements while Manual Welding," *IEEE Transactions on Cybernetics*, vol. 46, no. 11, pp. 2459–2472, 11 2016.

[5] A. Ajoudani, N. G. Tsagarakis, and A. Bicchi, "Choosing poses for force and stiffness control," *IEEE Transactions on Robotics*, vol. 33, no. 6, pp. 1483–1490, 12 2017.

[6] J. Woolfrey, W. Lu, and D. Liu, "A Control Method for Joint Torque Minimization of Redundant Manipulators Handling Large External Forces," *Journal of Intelligent and Robotic Systems: Theory and Applications*, vol. 96, no. 1, pp. 3–16, 10 2019.

[7] Y. Lai, S. Sutjipto, M. D. Clout, M. G. Carmichael, and G. Paul, "GAVRe 2 : Towards Data-Driven Upper-Limb Rehabilitation with Adaptive-Feedback Gamification," in *2018 IEEE International Conference on Robotics and Biomimetics, ROBIO 2018*. Institute of Electrical and Electronics Engineers Inc., 3 2019, pp. 164–169.

[8] S. Sutjipto, Y. Lai, M. G. Carmichael, and G. Paul, "Fitts' law in the presence of interface inertia," in *Proceedings of the Annual International Conference of the IEEE Engineering in Medicine and Biology Society, EMBS*, vol. 2020-July. Institute of Electrical and Electronics Engineers Inc., 7 2020, pp. 4749–4752.

[9] C. Ott, *Cartesian Impedance Control of Redundant and Flexible-Joint Robots*. Springer Berlin Heidelberg, 2008.

[10] H. Asada, "Dynamic analysis and design of robot manipulators using inertia ellipsoids," in *Proceedings - IEEE International Conference on Robotics and Automation*. Institute of Electrical and Electronics Engineers Inc., 1984, pp. 94–102.

[11] I. D. Walker, "Impact Configurations and Measures for Kinematically Redundant and Multiple Armed Robot Systems," *IEEE Transactions on Robotics and Automation*, vol. 10, no. 5, pp. 670–683, 1994.

[12] S. Sharma, M. Suomalainen, and V. Kyrki, "Compliant Manipulation of Free-Floating Objects," in *Proceedings - IEEE International Conference on Robotics and Automation*. Institute of Electrical and Electronics Engineers Inc., 9 2018, pp. 865–872.

[13] F. Vigni, E. Knoop, D. Prattichizzo, and M. Malvezzi, "The Role of Closed-Loop Hand Control in Handshaking Interactions," *IEEE Robotics and Automation Letters*, vol. 4, no. 2, pp. 878–885, 4 2019.

[14] M. G. Carmichael, R. Khonasty, S. Aldini, and D. Liu, "Human Preferences in Using Damping to Manage Singularities during Physical Human-Robot Collaboration," in *Proceedings - IEEE International Conference on Robotics and Automation*. Institute of Electrical and Electronics Engineers Inc., 5 2020, pp. 10 184–10 190.

[15] F. Ficuciello, L. Villani, and B. Siciliano, "Variable Impedance Control of Redundant Manipulators for Intuitive Human-Robot Physical Interaction," *IEEE Transactions on Robotics*, vol. 31, no. 4, pp. 850–863, 8 2015.

[16] J. J. Gil, Á. Rubio, and J. Savall, "Decreasing the apparent inertia of an impedance haptic device by using force feedforward," *IEEE Transactions on Control Systems Technology*, vol. 17, no. 4, pp. 833–838, 2009.

[17] O. Khatib, "A Unified Approach for Motion and Force Control of Robot Manipulators: The Operational Space Formulation," *IEEE Journal on Robotics and Automation*, vol. 3, no. 1, pp. 43–53, 1987.

[18] T. Yoshikawa, "Manipulability of Robotic Mechanisms," *The International Journal of Robotics Research*, vol. 4, no. 2, pp. 3–9, 6 1985.